Analyzing power in pion-proton bremsstrahlung, and the $\Delta^{++}(1232)$ magnetic moment

A. Bosshard, C. Amsler, M. Döbeli,* M. Doser,† M. Schaad,‡ J. Riedlberger,§ and P. Truöl
Physik-Institut der Universität Zürich, CH-8001 Zürich, Switzerland

J. A. Bistirlich, K. M. Crowe, S. Ljungfelt,** and C. A. Meyer††
Lawrence Berkeley Laboratory, University of California, Berkeley, California 94720

B. van den Brandt, J. A. Konter, S. Mango, and D. Renker
Paul Scherrer Institut, CH-5232 Villigen PSI, Switzerland

J. F. Loude and J. P. Perroud
Institut de Physique Nucléaire, Université de Lausanne, CH-1015 Lausanne, Switzerland

R. P. Haddock
Physics Department, University of California, Los Angeles, California 90024

D. I. Sober
Physics Department, Catholic University of America, Washington, D.C. 10024
(Received 22 January 1991)

We report on a first measurement of the polarized-target asymmetry of the pion-proton bremsstrahlung cross section ($\pi^+ p \to \pi^+ p\gamma$). As in previous cross section measurements the pion energy (298 MeV) and the detector geometry for this experiment was chosen to optimize the sensitivity to the radiation from the magnetic dipole moment of the $\Delta^{++}(1232)$ resonance μ_Δ. Comparison to a recent isobar model for pion-nucleon bremsstrahlung yields $\mu_\Delta = (1.62 \pm 0.18)\ \mu_p$, where μ_p is the proton magnetic moment. Since the asymmetry depends less than the cross section on the choice of the other input parameters for the model, their uncertainties affect this analysis by less than the experimental error. However the theory fails to represent both the cross section and the asymmetry data at the highest photon energies. Hence further improvements in the calculations are needed before the model dependence of the magnetic moment analysis can be fully assessed. The present result agrees with bag-model corrections to the SU(6) prediction $\mu_\Delta = 2\,\mu_p$. As a by-product, the analyzing power for elastic $\pi^+ p$ scattering at 415 MeV/c was also measured. This second result is in good agreement with phase shift calculations.

I. INTRODUCTION

Radiative pion-proton scattering (or pion-proton bremsstrahlung) experiments at energies near the $\Delta^{++}(1232)$ resonance can probe the magnetic moment μ_Δ of the Δ^{++}. Theoretical predictions for μ_Δ can be obtained from any model which predicts dipole moments for the baryons. In particular, the quark model predicts that the ratio of the magnetic moments of Δ and proton equals the ratio of their charges, $\mu_\Delta/\mu_p = e_\Delta/e_p$ [1]. Bag-model corrections to the quark model lead to modifications, e.g., the moment of the Δ^{++} ($\mu_\Delta = 2\,\mu_p$) is reduced by 17–20 % [2].

Because of the short lifetime of the Δ, its magnetic moment is not measurable with the usual spin-precession techniques. The alternative technique of using πp bremsstrahlung ($\pi p \to \pi p \gamma$) was proposed by Kondratyuk and Ponomarev already in 1967 [3]. These calculations recommended a particular kinematics with backward photon and forward pion and proton angles. There the external radiation from pion and proton interferes destructively and the experiments are most sensitive to the radiation from the Δ magnetic moment. Figure 1 illustrates this kinematical situation. The observed pattern can be understood classically [4]: a slowly moving particle radiates mainly transverse to its path, for a fast particle the intensity cones are Lorentz boosted in the forward direction. In the classical low-frequency limit the radiation from an accelerated charge decreases in intensity with ω^{-1}, while that from the magnetic moment increases with ω.

Previous pion-proton bremsstrahlung experiments measured a fivefold differential cross section $d^5\sigma/d\Omega_\pi\, d\Omega_\gamma\, dE_\gamma$ as a function of photon energy E_γ and tried to relate this cross section to the magnetic dipole moment of the Δ. The original predictions indicated that for values of $\mu_\Delta \approx 2\,\mu_p$, one should observe a very large bump in the $\pi^+ p\gamma$ cross section for intermediate

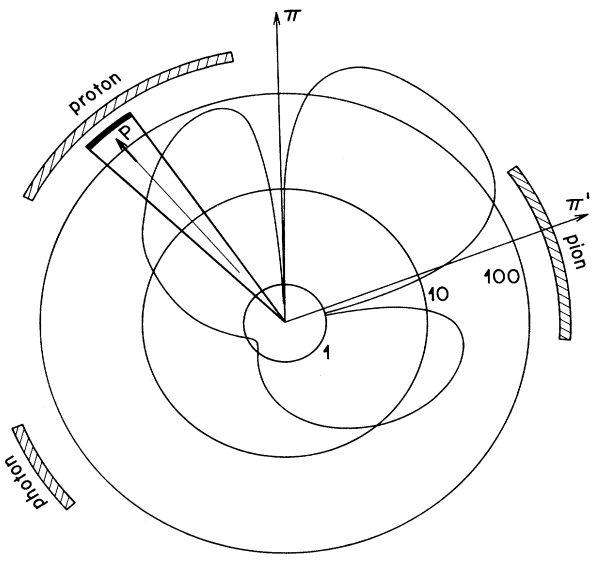

FIG. 1. External bremsstrahlung radiation pattern for 30 MeV photons, 300 MeV pions, and 70° pion scattering angle [5]. The proton direction varies within the limits indicated by the heavy circular segment. The intensity scale is logarithmic. The hatched areas indicate the detector position. The magnetic dipole moment radiation can be observed, where radiation from incoming and outgoing particles is minimal.

photon energies of 40 to 70 MeV [3, 6]. These predictions led to the first pion-proton bremsstrahlung experiments performed by the UCLA group at the Berkeley 184 inch cyclotron in the 1970's [7, 8]. These experiments found no structure in the cross section other than the expected $1/E_\gamma$ falloff from external bremsstrahlung. The complete data set taken at three pion energies (269, 298, and 324 MeV) for both positive and negative pions proved rather difficult to interpret in terms of the magnetic dipole moments of the Δ within the existing models, as extensively discussed by the UCLA group [8]. It became clear at that time however, that for $\pi^+ p\gamma$ a near cancellation of all magnetic moment contributions occurs only for $\mu_{\Delta++} \approx 2\mu_p$. This was first pointed out by Musakhanov [9], whose isobar model analysis using PCAC (partial conservation of axial-vector current) and neutrino data to fix model parameters actually lead to the value $\mu_{\Delta++} = (1.3 \pm 0.6)\ \mu_p$ based on the earliest UCLA data [7]. Furthermore, an analysis restricted to those photon energies where the final Δ^{++} mass is at the peak of the resonance and to backward photon angles was presented together with the experimental data [8], yielding $1.7 < \mu_{\Delta++}/\mu_p < 2.4$. This analysis was suggested by Pascual and Tarrach [10], who confirmed Musakhanov's [9] observation concerning the cancellation and designed a formalism, which allowed to derive qantitative limits for μ_Δ from the observed cross section for the restricted kinematics mentioned above. Only in the mid 1980's a dynamically consistent and gauge-invariant model for πN bremsstrahlung was developed at MIT, which achieved a satisfactory fit to all the existing UCLA data with $2.5 < \mu_\Delta/\mu_p < 3.5$ [11].

The MIT theory [12] is an isobar model which is fitted to experimental $\pi^+ p$-phase shifts. The model includes $P33$, $S31$, and $P31$ partial waves. The $\pi N\Delta$ vertex is parametrized as

$$f_{\pi N\Delta} h(q^2) = \frac{g m_\pi}{(1 + q^2/\alpha^2)^n} ,$$

giving two free parameters g and α for each partial wave and a given n. In addition a mass parameter (m_Δ) appears in the spin-$\frac{3}{2}$ propagator G_Δ,

$$G_\Delta = (E - m_\Delta - \Sigma_\Delta)^{-1} ,$$

where Σ_Δ is a self-energy correction. The free parameters obtained from fitting are shown in Table I. For the $P33$ wave, two different sets of parametrizations are possible. This ambiguity leads to cross sections which differ up to a factor of 2 in the kinematical region where the sensitivity to μ_Δ is largest, and consequently to a large uncertainty in the value of μ_Δ. However, it was also shown in this model calculation that a measurement of the polarized-target asymmetry of the bremsstrahlung process would still be sensitive to μ_Δ, but quite insensitive to the choice of the $P33$ parametrization. It was this prediction which motivated our polarized-target experiment. The MIT-model results, which entail a nonrelativistic treatment of the $\pi N\Delta$ and the $N\gamma$ vertex function, were later confirmed to a large extent by Wittman [13], who developed a fully relativistic isobar model. The overall agreement with the UCLA data [8] is similar with $2.0 < \mu_{\Delta++}/\mu_p < 2.7$.

An asymmetry measurement is technically even more difficult than a cross-section measurement, since it is not possible to polarize pure hydrogen, and the additional bound protons in the target further enhance the already high background. Therefore we first did a cross-section measurement with an unpolarized liquid hydrogen target. It showed that the detection of all three particles in the final state with sufficient resolution would allow us

TABLE I. Parameters of the MIT theory.

Partial wave	α	g	m_Δ	n
$P33$	$1.20\,\mathrm{fm}^{-1}$	$2.12\,m_\pi^{-3/2}$	1445 MeV	$n = 1$
$P33$	$2.20\,\mathrm{fm}^{-1}$	$1.79\,m_\pi^{-3/2}$	1332 MeV	$n = 2$
$S31$	$5.75\,\mathrm{fm}^{-1}$	$0.36\,m_\pi^{-1}$		
$P31$	$2.09\,\mathrm{fm}^{-1}$	$2.74\,m_\pi^{-2}$		

to eliminate nearly all background. This measurement has been described elsewhere [14]. It could be described by the MIT theory with $2.3 < \mu_\Delta/\mu_p < 3.3$, but discrepancies between theory and data appeared at backward pion angles. The present paper describes the polarized-target experiment and reports the bremsstrahlung analyzing power. As a by-product, the analyzing power for elastic πp scattering was also determined, with good agreement with previous results at nearby energies. A brief summary of the polarized-target results was given earlier [15].

II. EXPERIMENTAL SETUP

The setup was essentially the same as in the cross-section part of this experiment [14]. All three final particles (π^+, p, and γ) were detected in three detectors, but the liquid hydrogen target was replaced with spin polarized protons. Figure 2 shows the setup seen from above: the π^+ entered from the left, through the last quadrupole magnet (QSK), a steering magnet (SSK), and lead shielding (S), and encountered the target (T). The magnetic field around the target, pointing in vertical direction, deflected the beam by 7.8°. Scattered pions fired trigger counters (E), had their tracks recorded by four wire chambers ($M1$–$M4$) in the magnetic spectrometer (AEB) and triggered one of eight pairs of scintillators (B and A). Scattered protons left position and energy-loss information in a hodoscope (H) and stopped in one of three scintillators (P), or were vetoed if they reached anticounters (V) behind. The sodium iodide array (NaI), which analyzed the photons, was guarded against charged particles by anticounters (AC) and protected by shielding (S). A scintillator telescope (J_1J_2) and another counter (π_1) monitored beam intensity.

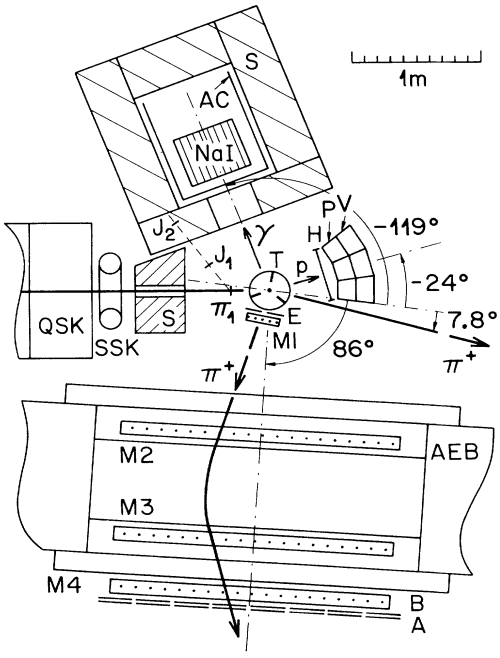

FIG. 2. Experimental setup.

A. Target

The polarized-proton target consisted of 8 cm^3 of frozen butanol beads ($C_4H_{10}O$), 1–2 mm in diameter, and cooled to 0.5 K in liquid ^{3}He [16]. The hydrogen nuclei of the butanol were dynamically polarized in a 2.5 T magnetic field. Spin polarizations of typically +58% and −47% were achieved by applying appropriate microwave frequencies of 70.580 and 70.200 GHz, respectively. The polarization was measured every 20 minutes by nuclear magnetic resonance methods using a fast sweep Q meter, calibrated against the proton polarization signal at thermal equilibrium. The temperature measurement limited the relative accuracy of the calibration to 5%. The butanol beads were kept in a cylindrical copper cavity with 0.05 mm walls and 22 mm diameter. A dummy target, containing 9 g of carbon immersed in liquid ^{3}He, was mounted just below in a cavity of the same type. It could be raised to the beam center for background measurements. There was nearly the same amount of helium in both targets.

B. Pion spectrometer

The scattered pions at angles near 90° were analyzed in a magnetic spectrometer that had formerly served as a pair spectrometer [14, 17]. The small vertical aperture of the window-frame magnet defined an almost coplanar geometry (±7° out of plane, Table II). The accepted solid angle was ≈ 125 msr. Four wire chambers ($M1$–$M4$) surveyed the pion tracks. The positions of the chambers were measured to an accuracy of ±1 mm and were checked by analyzing straight-through tracks, i.e., pion tracks with the magnetic field off. Each wire chamber had three planes and the spacing between wires was 2 mm.

The field at the center of the spectrometer magnet was 6497.2 G and was monitored with a Hall probe. Field deviations (<0.9 G) and errors in the field map were insignificant. An array of two plastic scintillators E just in front of the first wire chamber started all time-of-flight measurements [time-to-digital converters (TDC's)] and triggered the pion spectrometer together with another array of 2×8 scintillators (B, A) behind the last chamber. Both arrays were equipped with pulse height measurement [analog-to-digital converters (ADC's)] and the pion time of flight from E to the AB pairs was also recorded.

The procedure used to relate hits in the chambers to pion momentum was the following: The wire positions and a field map were input to a Monte Carlo program that tracked about 18 000 pions through the spectrometer. The initial four-momenta of these pions and the corresponding wire numbers were submitted to a principal components analysis [18]. Hermite or Chebychev polynomials in the principal components were fitted to the momenta of the particles and the interaction points.

TABLE II. Accepted momenta and angles for bremsstrahlung (elastic) events and detector resolutions plus some other experimental parameters (laboratory system). Momentum is p, α and β are horizontal and vertical angles. Values for the carbon dummy target in curly brackets.

		Acceptance or range Low	High	Resolution or error σ
π	p (MeV/c)	160 (250)	300 (320)	3.0 (3.5)
	α (deg)	68 (68)	110 (110)	1.7–0.8 {1.8–0.9}
	β (deg)	−7 (−7)	7 (7)	0.7–0.2 {0.9–0.4}
p	p (Mev/c)	400 (410)	550 (570)	8.1–9.3 {14.6–15.3}
	α (deg)	−6 (−22)	−42 (−46)	1.71 {1.77}
	β (deg)	−10 (−10)	10 (10)	1.64 {1.69}
γ	p (MeV/c)	20	125	3.0–4.9
	α (deg)	−129	−109	1
	β (deg)	−10	10	1
Beam	p (MeV/c)	414.6, T=298 MeV {411.6}		1.4 {1.9}
	α (deg)	0		0.73 {0.75}
	β (deg)	0		0.41 {0.45}
Target polarization		−0.47	0.58	5%

The Monte Carlo coefficients were then used for real data. The pion momentum and angles could be calculated by first transforming the wire hits into principal components and then evaluating the corresponding polynomials [14, 17, 19]. A two-dimensional target traceback could be obtained with this method, too. However, a straight line through the first two chambers, neglecting the curvature of the pion path, was accurate enough. The exact position of the interaction point was unknown, because no second particle was traced back. An average path through target and target field had to be assumed, leading to an error in momentum and angle. This, together with multiple scattering, limited the angular resolution (Table II). The polynomial fit contributed $\Delta p/p$=0.01 to the momentum resolution [14].

C. Proton detector

The protons were analyzed in forward direction with three 15 cm thick scintillator blocks P, read out with photomultipliers on top and ADC's for energy measurement [20]. Particles escaping the blocks were vetoed by a second row of scintillators V. Energy loss, time of flight and direction of the proton were determined with a twelve-strip hodoscope H. The horizontal direction was obtained from the strip number including an energy dependent correction for the deflection in the target field ranging from 5.7° (at T=160 MeV) to 8.0° (at T=80 MeV). The variation of this correction with energy was small compared to the 4.4° width of a hodoscope strip. The strips were viewed by 19 mm diameter phototubes on both ends. Vertical elevation of the proton hit was reconstructed from the time difference of the TDC signals from the two tubes. This elevation measurement had been calibrated with a radioactive source. Total-energy and dE/dx measurements were calibrated with protons from elastic πp scattering: the pions were analyzed and the proton energies were calculated kinematically. Linear relations between deposited energy and ADC readings were established. The detector stability was monitored by sampling elastic πp events with a pion in a narrow angle and momentum band, and hence the proton in narrow energy band. The calibration coefficients were adjusted if the monitor signals drifted. The calibrations were repeated several times during the experiment. Light from a light-emitting-diode (LED) pulser was fed to all three energy blocks and was used to monitor the most forward block, because no protons from elastic scattering in coincidence with pions were seen in this block (Fig. 3, at $E_\gamma = 0$). For calibration of this block, the proton detector was rotated to more backward angles. The stability of the light pulser signal assured that this calibration was rate independent. At its forward position, the block accepted a rate of 10^6 particles per second from the beam halo. In fact it was this rate which prevented us from increasing the incident pion flux and from moving to more forward proton angles, and therefore limited the acceptance at high photon energies. Errors in the energy measurement arose from uncertainties in energy loss corrections, accuracy of the calibration adjustments and a 1% contribution from the scintillator resolution (Table II). The latter contribution was determined from the kinematic fit (Sec. III B) to elastic events by comparing the "improved," fitted energy to the initial measurement from the ADC reading. The changes in proton energy follow a Gaussian distribution if the resolutions are correctly entered into the fit [21].

D. Photon detector

Photons were detected at backward angles, relative to pion and proton. An array of 8×8 NaI(Tl) crystals, each 63.5×63.5×406 mm^3 (15.4 radiation lengths long), covered a 50.8×50.8 cm^2 area at 101 cm from the target. The detector was wrapped in 35 cm thick shielding, made of borated polyethylene and lead [22]. Scintillators guarded against charged particles (backscattered or cosmic) on five sides. The trigger electronics accepted all possible combinations of 2×2 adjacent crystals and fired the detector when more than about 15 MeV was

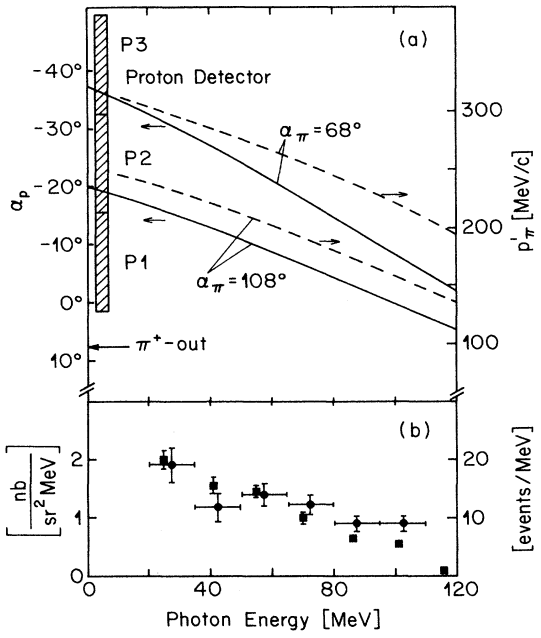

FIG. 3. (a) Proton emission angle relative to the incoming pion direction at the target. The average energy loss in the target and the deflection in the magnetic field of the target is taken into account. The direction of the unscattered outgoing pions and the position of the three proton detectors is indicated (left scale and solid lines). Outgoing pion momenta are given too (right scale and dashed lines). The upper and the lower curves correspond to the limits of the pion spectrometer acceptance. (b) Cross section measured with a liquid hydrogen target [14] ($75° < \alpha_\pi < 95°$)(left scale, •) and number of events measured in the present experiment with a polarized target, not corrected for acceptance losses (right scale, ■, offset by 2 MeV).

deposited. There were attenuators (factor of 10) in all 64 ADC channels and each individual crystal could be calibrated with sources (^{88}Y and ^{137}Cs) with the attenuators switched off. A further calibration point at 29 MeV from cosmic muons was also used [22]. Calibrations were done typically twice per week during the 32 days of data taking. The energy resolution of the crystal ensemble was tested with the 129.4 MeV photon line from the reaction $\pi^- p \to \gamma n$. The linewidth was σ=5.0 MeV, indicating about 40% deterioration of the light collection compared to earlier use in a $\pi^+ \to e^+ \nu_e \gamma$ decay experiment [23]. The energy resolution can be parametrized as $\sigma - 0.018(129 - E_\gamma)$, where E_γ is the energy in MeV [22]. The crystal containing the largest part of the electron-photon shower essentially determined the photon direction. The spatial resolution could only be slightly improved by calculating an energy-weighted average over all bars that had been struck [22].

E. Detector resolution and acceptance

Table II lists various detector parameters, including the resolution of the three arms. Lower and upper limits are given where it was necessary to parametrize the resolution as a function of the particle energy or momentum. The angular coordinates used in Table II are α, the particle direction measured in the horizontal plane, relative to the direction at the interaction point of the incoming pion, and β, the elevation out of that plane. The limits in angular and momentum acceptance for bremsstrahlung and elastic events are also given. The detector acceptance was not exactly limited by square boundaries, but it will be demonstrated in Sec. IV C that the limits given in Table II suffice for comparison with future theoretical calculations. Figure 3 indicates that beyond 100 MeV the photon energy acceptance begins to decrease because protons miss the proton detector near the forward direction and because more pions decay before they are detected. Since the acceptance cancels in the evaluation of the cross-section asymmetry, it does not need to be known (Sec. IV B).

F. Pion beam

The polarizing field around the target deflected the beam by 7.8° as determined from the field map with a Monte Carlo tracking routine and checked with elastic scattering events, where the kinematics is overdetermined.

The beam momentum was measured using the time-of-flight difference of pions and protons in the beam. These are simultaneously produced at 19.75 ns intervals (50.63 MHz accelerator radio frequency) at the production target. Normally the protons were ranged out by a 6 mm carbon absorber, placed before the first bending magnet. If this absorber was taken out, pions and protons of the same momentum reached the experiment, where a small fraction was registered with a tiny scintillator. The scintillator signal stopped a TDC that had been started with every fifth pulse from the cyclotron frequency. The TDC was calibrated with the 19.75 ns time difference that separated the five pion peaks, or the five proton peaks, that appeared in its time spectrum and a time-of-flight difference $\Delta\tau$=8.929 ns between pions and protons was determined with 0.7% accuracy. The beam momentum at the production target was determined by comparing the measured time difference to the one expected near 420 MeV/c:

$$p = 420 \text{ MeV}/c + (\Delta\tau - \Delta\tau_{420})/(\partial\Delta\tau/\partial p) , \qquad (1)$$

The length of the beamline and the position and thickness of all vacuum windows had to be considered, and insensitivity of the TDC to pulse height had to be guaranteed to compute the expected time with $\Delta\tau_{420} = 6.86$ ns $\pm 3.3\%$ and $\partial\Delta\tau/\partial p = -0.283$ ns/(MeV/c). Corrected for energy loss, the momentum p was 414.6 MeV/c at the target center, with a systematic error of $\pm$ 0.9 MeV/c (Table II). The momentum spread was calculated to be $\pm$ 1.2 MeV/c, using a ray tracing program and the known slit settings.

At low intensities the scintillator π_1 (Fig. 2) intersected and monitored the beam. It could however not be operated at typical rates of 40×10^6 π^+/s during the

experiment. A scintillator telescope J_1J_2 was installed which monitored beam flux by counting pions backscattering from π_1. The telescope was calibrated against π_1 at low-beam intensities.

G. Trigger and data taking

The individual trigger signals from the three detectors could be combined to trigger on bremsstrahlung ($\pi p\gamma$) or on elastic (πp) events. All information was collected by a PDP 11/40 computer via a CAMAC interface and was written to magnetic tapes for later off-line analysis. One elastic run for every five bremsstrahlung runs was taken, and the polarization of the butanol target was switched about once a day. Measurements on the dummy carbon target were made at five times during the experiment.

III. DATA REDUCTION

Out of the 2×10^6 bremsstrahlung triggers recorded on tape, only about 1400 were genuine $\pi^+p\gamma$ events. Most of the triggers arose from elastic π^+p scattering events in coincidence with a random photon. True events were selected with a kinematic fit. The random background events were checked with pion-proton pairs coinciding with a photon from a preceding or subsequent beam pulse. As evident from the photon time spectrum (Fig. 4), the random contribution under the real timing peak is quite high. The events not contained in any of the peaks are associated either with neutrons or with positrons from the $\pi^+ \rightarrow \mu^+ \rightarrow e^+$ decay chain, started by a pion scattered into the photon detector. The in-time photons stem mainly from charge exchange $\pi^+n \rightarrow \pi^0p$ on bound nucleons in coincidence with a second pion in the beam pulse causing an elastic scattering event, and from $\pi^+p \rightarrow \pi^+p\pi^0$.

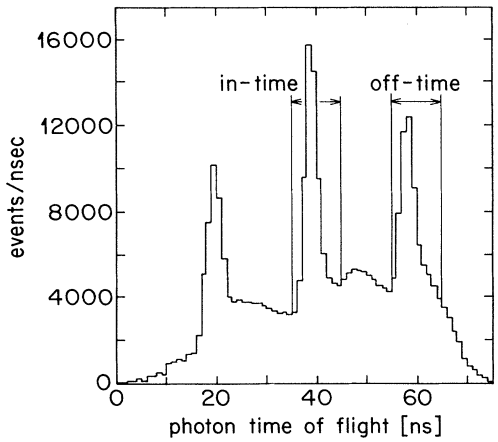

FIG. 4. Photon time spectrum. Photons correlated in time with the pion and the proton were in the central peak, photons from the previous or the next beam pulse in the side peaks. Uncorrelated background stemmed from Michel positrons at the end of the decay chain of backscattered pions ($\pi^+ \rightarrow \mu^+\nu$, $\mu^+ \rightarrow e^+\nu\bar{\nu}$), from slow neutrons, etc. Photons from the "off-time" window served for background estimation.

A. Event reconstruction

In the off-line analysis, protons in the pion spectrometer were suppressed by cuts on time of flight and pulse height. The four wire chambers were then searched for multiple hits and up to three pions per event were reconstructed. Each wire chamber had three wire planes, so that a pion could be reconstructed even if one of the planes had not reported. The efficiency of a wireplane was calculated from the number of times the plane had been missing in a good pion event. The efficiency of all four chambers together was typically 70%. A target traceback cut removed events from vacuum windows and heat shields. In the proton detector, the energy loss measurement from the hodoscope was used to suppress pions. The hodoscope was too close to the target to separate pions from protons by time-of-flight cuts. A photon time cut was necessary to pick only photons correlated in time with the pion and the proton (Fig. 4). Random background was analyzed by combining pion-proton pairs with photons from a neighboring beam pulse. The carbon target was analyzed likewise.

Elastic pions, i.e., pions from the reaction $\pi p \rightarrow \pi p$ with a free target proton, could easily be spotted by comparing the reconstructed pion momentum to the momentum of an elastic pion going in the same direction (Fig. 3). For bremsstrahlung pions the measured momentum was lower, and in a bremsstrahlung analysis most elastic events were removed with a cut above $p_\pi - p_\pi(\text{elastic}) = -6$ MeV/c (Fig. 5).

After that cut, the bremsstrahlung events emerged in the spectra of other kinematical quantities: these were for instance the energy balance

$$E_{\text{bal}} = (E_{\text{in}} + m_p) - (E_\pi + E_p + E_\gamma) \qquad (2)$$

or the "target mass"

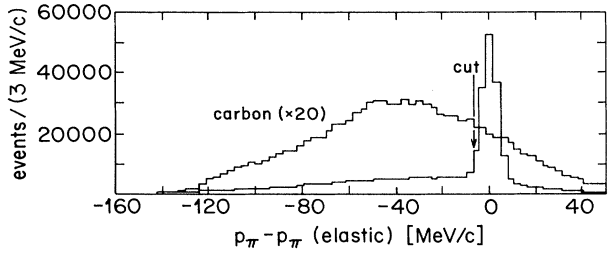

FIG. 5. Measured pion momentum minus the momentum of an elastic pion going in the same direction. About half of the events that had a pion, a proton, and a photon reconstructed were elastic πp scattering in coincidence with a random photon. Most of these were removed with a cut above -6 MeV/c. There were no free protons in the carbon target and no elastic signal is seen in the carbon spectrum. The carbon scale is magnified (×20).

$$m_t = \sqrt{(E_{\rm in} - E_\pi - E_p - E_\gamma)^2 - (\mathbf{p}_{\rm in} - \mathbf{p}_\pi - \mathbf{p}_p - \mathbf{p}_\gamma)^2} \quad (3)$$

where E and $\mathbf{p}$ are energies and momenta of the incoming and outgoing particles. For true bremsstrahlung events, where the incoming pion had interacted with a *free* proton, $E_{\rm bal}$ should be zero (Fig. 6) and m_t should equal the proton mass m_p (Fig. 7).

B. Kinematic fit

The experiment measured the direction, and momentum or energy of all three outgoing particles. With the known momentum of the incoming pion and the assumption of a free proton target, the kinematics was overdetermined and the measured quantities generally did not satisfy energy and momentum conservation, either because it was not a true event, or because the measurements were not infinitely accurate. A kinematic fit was performed. Figure 8 shows the confidence level (C.L.) distribution, which should be uniform for the true events. False events appeared at low C.L.'s. In the final data set, only events with C.L.>0.2 were included. This implies that 20% of the true events were lost by this cut [24].

All events that had passed the cuts from the previous section were submitted to a kinematic fit and were entered into a three-dimensional histogram with the dimensions C.L., pion angle, and photon energy. For each run, this histogram together with other information like scalers, wireplane efficiencies, average target polarization, number of events that had passed the various stages of the analysis, etc., were appended to a database. This database allowed fast calculation of A at confidence levels other than 0.2 and, if desired, with restricted pion angles, without reanalysis of the tapes.

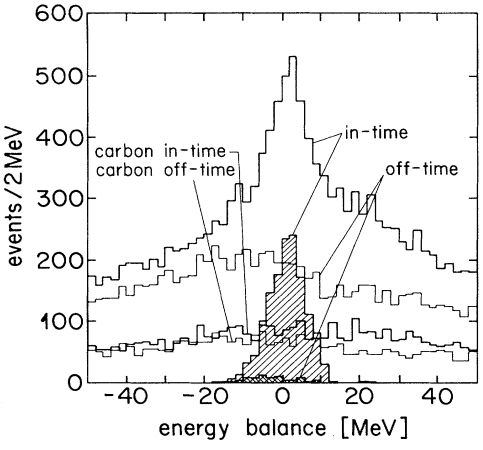

FIG. 6. Energy balance $E_{\rm bal}$, before and after the C.L. cut of Fig. 8. Bremsstrahlung events were in the peak around zero. For the background data (πp pairs with an off-time γ) the signal was absent (32 events with $E_\gamma > 20$ MeV survived the C.L. cut, Table III) The carbon spectra for in-time and off-time photons were the same; there was no indication of an enhanced in-time signal around zero. Carbon spectra are given before the C.L. cut.

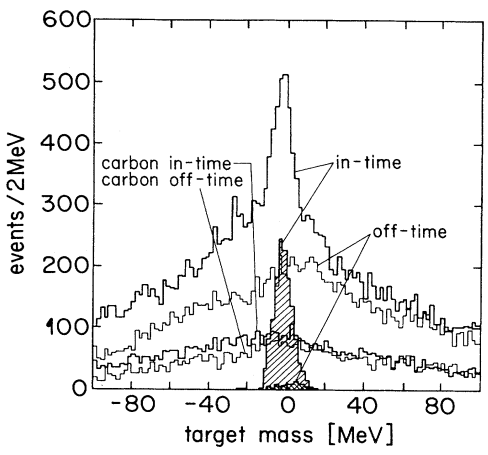

FIG. 7. Distribution of reconstructed target mass minus proton mass, $m_t - m_p$. The histograms are otherwise as in Fig. 6. Again, the bremsstrahlung events appear in the peak at zero.

C. Bremsstrahlung backgrounds

As apparent from Fig. 8 and Table III, the number of background events was quite low after the confidence level cut. The total number of random events is only 3%, concentrated in the two lowest photon energy bins. For the carbon dummy target the number of events surviving the confidence level cut is consistent with zero after random subtraction. We believe that these random events and dummy target data provide a good estimate of

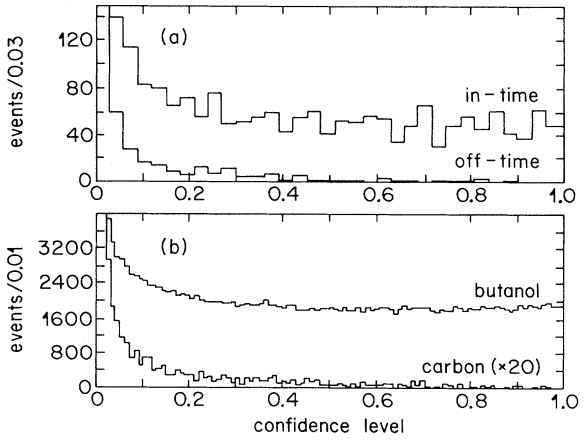

FIG. 8. (a) Confidence level (C.L.) distribution for bremsstrahlung triggers (after the cuts from Sec. III A). 92% of all entries were in the lowest bin. The true data sample (in time) is compared to the background sample (off time). The C.L. cut was at 0.2. (b) C.L. distribution for πp events, for butanol and carbon. The carbon scale is magnified (×20).

TABLE III. Statistics for the bremsstrahlung analysis. Beam flux (including corrections) is given in arbitrary units for negatively (−), positively (+), and unpolarized (0) target. The events that had a pion and a proton, and a photon in the correct time window are labeled "good $\pi p\gamma$." These events were passed to the "elastic cut" (Fig. 5). Good bremsstrahlung events (C.L. > 0.2, $E_\gamma > 20$ MeV) were found in the data sample with the prompt photons (in time), some fake events survived in the sample with an out-of-time photon (off time), and also in the data from the carbon dummy target.

		Butanol		Carbon	
		In time	Off time	In time	Off time
No. of runs		76		14	
Flux α	−	339			
	+	271			
	0	20			
Flux α total		630		120	
Triggers		2.12×10^6		4.83×10^5	
Good $\pi p\gamma$		43 300	39 300	8140	6730
After elastic cut		23 300	15 000	6870	5520
C.L.>0.2	−	681	18		
	+	436	14		
	0	27	0		
C.L.>0.2 total		1144	32	11	9

the background in the polarized target data, for reasons which we will now discuss briefly.

True background coincidences (with an identified pion-proton pair) could arise from $\pi^+p \rightarrow \pi^+p\pi^0$, from $\pi^+p \rightarrow \pi^+p\gamma$ on a bound nucleon, and from the breakup of a bound quasideuteron $\pi^+M(Z,A) \rightarrow \pi^+pnM(Z-1,A-2)$ with the neutron misidentified as a photon.

As shown in our previous paper dealing with liquid hydrogen [14], π^0 production can easily be removed by kinematical considerations. In our present experiment (with more backward pions on average), the relevant protons are missing the proton detector in most cases. Bremsstrahlung on bound protons can be measured with the dummy target which contains ^{12}C and ^{3}He (with binding energies of 16.0 and 5.5 MeV). Our resolution on the reconstruction of the target mass is σ=4.3 MeV (Fig. 7) sufficient to remove this background. The butanol target contains 8% oxygen atoms (binding energy 12.1 MeV) not present in the dummy target, for which the same statement can be made.

Slow neutrons are removed by the photon time-of-flight cut, and for fast neutrons it is hardly possible to balance energy and momentum. Furthermore this signal should be present in the dummy target.

The random contributions could be checked with the analysis of the neighboring photon time peaks. Their primary source is π^+p elastic scattering with a random photon, for which the kinematical constraints can be fulfilled only for low photon energies and with both the pion and the proton in the tails of their resolution functions. For the second class $\pi^+n \rightarrow \pi^0p$, $\pi^0 \rightarrow \gamma\gamma$ in coincidence with a scattered π^+ on a bound or free proton from a second pion in the same beam burst (35% probability), the photon energies are quite high and kinematical cuts easily remove these events. If the random π^+ is coming from a bound proton or neutron, this contribution should be observed with the dummy target, too. If the pion is scattered by a proton, the elastic cut already removed this type of event. Lastly, the decay of a scattered π^+ into a μ^+ within the pion spectrometer, leading to an apparent lower pion momentum, could be accompanied by a random photon. This type of event should (a) be contained in the random sample and is thus subtracted and (b) normally fails the kinematical reconstruction (except at very low photon energies), as checked by Monte Carlo simulation [14].

As a further check we have given in Fig. 3 the number of events observed, summed over both spin directions versus photon energy. The results agree quite well with the unpolarized data, bearing in mind that no attempt has been made to correct for the acceptance loss at the very high photon energies.

IV. RESULTS

This section defines the analyzing power and describes how it was calculated as the solution of an ordinary maximum likelihood problem. Results for bremsstrahlung and elastic scattering are given.

A. Definition of analyzing power A

The analyzing power, which we want to measure is defined as

$$A = \frac{\sigma(+) - \sigma(-)}{\sigma(+) + \sigma(-)} . \tag{4}$$

$\sigma(+)$ and $\sigma(-)$ refer to the cross sections for proton spin eigenstates $|+\rangle$ and $|-\rangle$, and spin components $\sigma_z = \boldsymbol{\sigma} \cdot \mathbf{n}$, where $\mathbf{n}$ is a unit vector defined with the momenta of the incoming and the scattered pion, $\mathbf{n} = \mathbf{p}_{in} \times \mathbf{p}_\pi / |\mathbf{p}_{\rm in} \times \mathbf{p}_\pi|$.

Positive scattering angles are associated with $\mathbf{p}_\pi$ [25].

For a target with polarization $\langle\sigma_z\rangle = P$, a cross section,

$$\sigma(P) = \sigma(0)(1 + AP) \ , \tag{5}$$

will be measured. $\sigma(0) = \frac{1}{2}[\sigma(+) + \sigma(-)]$ is the cross section for an unpolarized target.

The number of events k that will be observed in a measurement is proportional to the cross section and proportional to the number of incoming pions (beam flux α). With background proportional to beam flux one has

$$k = E\alpha(1 + AP) + B\alpha \ . \tag{6}$$

The background B can be determined from the number of events b found in the background data sample, $B\alpha = b$. The two other unknowns A and E then can be found from two measurements at two different target polarizations P_+ and P_- by solving the equations

$$k_+ = E\alpha_+(1 + AP_+) + B\alpha_+ \ , \tag{7}$$

$$k_- = E\alpha_-(1 + AP_-) + B\alpha_- \ . \tag{8}$$

The result for A is

$$A = \frac{\alpha_- k_+ - \alpha_+ k_-}{\alpha_+ P_+ k_- - \alpha_- P_- k_+ - (P_+ - P_-)\alpha_+\alpha_- B} \ . \tag{9}$$

Here it was assumed that background B is polarization independent, i.e., that $b_+ = B\alpha_+$ and $b_- = B\alpha_-$ for the two background data samples. For the ideal experiment, with $\alpha_+ = \alpha_-$, $P_+ = 1$, $P_- = -1$ and no background, Eq. (9) reduces to $A = (k_+ - k_-)/(k_+ + k_-)$.

B. Likelihood fit

The calculation of A was complicated by a continuous, 10% overall decrease of the polarization amplitudes P_+ and P_- due to radiation damage in the target, and by variations in wire chamber efficiencies. Therefore, an average polarization P_i was calculated for each run and α_i was defined as the product of beam flux and chamber efficiency for that run. All other detector efficiencies as well as the solid angle are contained in the factor E (and B) and need not be known as long as they are not changing. The probability of observing k_i events in run number i is given by Poisson statistics,

$$W_i = \frac{\lambda_i^{k_i}}{k_i!} \exp(-\lambda_i) \ , \tag{10}$$

where λ_i is the number of events that is to be expected for run number i,

$$\lambda_i = E\alpha_i(1 + AP_i) + B\alpha_i \ . \tag{11}$$

This is identical to Eq. (6), except that there the expectation value was already replaced by the best guess, namely k_i. The expectation value for the number of background events b_j in run j is

$$\lambda_j = B\alpha_j \ . \tag{12}$$

The probability of observing exactly $(k_1, \ldots, k_N)$ events in N runs and $(b_1, \ldots, b_M)$ events in M background runs is the product of all W_i and W_j:

$$\mathcal{L} = \prod_i W_i \prod_j W_j \ . \tag{13}$$

The likelihood function $\mathcal{L}$ depends on the unknown parameters A, E, and B. A maximum likelihood fit determines a set (A, E, B) that maximizes $\mathcal{L}$. The search for the maximum and the estimate for the parameter errors used standard program packages [26]. The errors of the α_i were neglected. Equation (9) suggests that A is roughly proportional to $1/P$. So a 5% error was added linearly to the statistical error of A, to account for the 5% calibration error in the polarization P. Equation (9) is the maximum likelihood result for A in the special case of only two runs.

C. Bremsstrahlung analyzing power

Figure 9 shows the analyzing power A for the $\pi p \to \pi p\gamma$ process in 15 MeV photon energy bins from 20 to 125 MeV compared to the MIT theory. Theoretical curves were obtained with a Monte Carlo program that took actual detector acceptances into account, using the code from the MIT group [27] to compute the differential cross sections $\sigma(+)$ and $\sigma(-)$. From about 2500 simulated events, theoretical asymmetries were calculated for several values of μ_Δ.

To determine which μ_Δ best fits the data, a χ^2 fit was performed. Dropping the last data point at $E_\gamma = 117.5$ MeV, this χ^2 was minimal for

$$\mu_\Delta = 1.62 \pm 0.18 \ \mu_p \tag{14}$$

(Fig. 10), where μ_p is the magnetic moment of the proton ($\mu_p = 2.793\, e\hbar/2m_p$). Table IV lists the results for both MIT models, with fits which include between three and all seven data points. Representative curves are shown in Fig. 9. The predicted decrease in $|A|$ at the highest energies, where the theory may be no more applicable [11], does not seem to be confirmed by the data.

The predicted A is independent of μ_Δ at both low and high photon energies. At $E_\gamma = 60$ MeV, the final-state

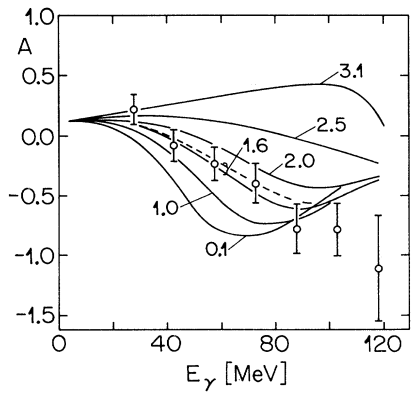

FIG. 9. Bremsstrahlung polarized-target asymmetry versus photon energy. The curves are predictions from the MIT theory for several values of μ_Δ. The dashed curve is for model II (see text for explanation).

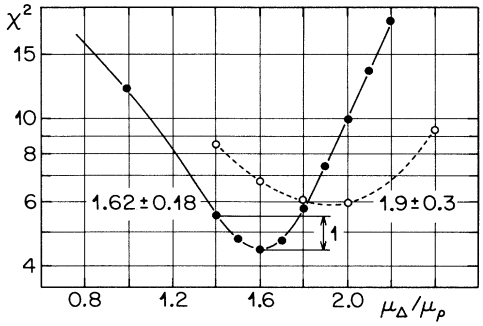

FIG. 10. χ^2 fit of the bremsstrahlung asymmetry to the MIT theory. χ^2 is a minimum for $\mu_\Delta = 1.62 \pm 0.18\,\mu_p$ with five degrees of freedom ($E_\gamma < 110$ MeV). A fit to the cross section from our previous experiment [14] (dashed curve) agreed with this result if photon energies were restricted to $E_\gamma < 80$ MeV and pion scattering angles to $75° < \alpha_\pi < 95°$.

π^+p system is at the peak of the Δ mass distribution and the sensitivity maximal. This is why the result of the fit does not depend too strongly on the upper limit of the fit, even though the χ^2 gets worse (Table IV). At low energy the Low soft-photon theorem [28] assures that the analyzing power for bremsstrahlung is tied to that for elastic scattering.

The present result for μ_Δ is not consistent with the value $\mu_\Delta = 2.8 \pm 0.5\,\mu_p$, that was extracted from our cross-section measurement [14]. A repeated fit to our published cross-section data [14], with the photon energies restricted to less than 80 MeV (four data points), where the theory should be more reliable, and pion angles between 75° and 95°, overlapping with the present polarized target data, yielded $\mu_\Delta = 1.9 \pm 0.3\,\mu_p$ for model I and $(1.8 \pm 0.3)\,\mu_p$ for model II and hence diminished the discrepancy.

The results are tabulated in Table V, with which the analyzing power could be calculated using Eq. (9). All results quoted come from the likelihood fit, however, which also included a few unpolarized runs ($P_i = 0$) and did not use the average polarizations P_-, P_+. Our experimental results are compared here to the MIT predictions. For future comparison with other theories, the approximate detector acceptance, given in Table II, can be used. We also performed a "point calculation," i.e., we calculated the theoretical asymmetry for a fixed geometry at the average pion and photon angles (Table V, caption and last column), and compared it to the correctly averaged result (Table V, second last column). The deviations are small.

TABLE IV. Results of the χ^2 fits of the MIT theory to the measured analyzing powers. For MIT models I and II, and with restriction to low photon energies.

Deg. of freedom	E_γ (MeV)	Model I χ^2	Model I μ_Δ	Model II χ^2	Model II μ_Δ
2	<65	1.1	1.66 ± 0.27	1.1	1.54 ± 0.32
3	<80	1.2	1.71 ± 0.20	1.1	1.59 ± 0.24
4	<95	2.0	1.64 ± 0.19	2.1	1.50 ± 0.21
5	<110	4.4	1.62 ± 0.18	4.0	1.46 ± 0.19
6	<125	7.2	1.59 ± 0.17	6.6	1.46 ± 0.17

D. Elastic analyzing power

As already mentioned, most of the bremsstrahlung triggers arise from elastic $\pi^+p \to \pi^+p$ scattering in coincidence with a random photon. Furthermore a considerable amount of data was taken with an elastic πp trigger. These elastic events were easily analyzed with the same programs and the asymmetry could be calculated.

All events with an identified pion and proton were analyzed under the elastic scattering hypothesis. Kinematical quantities, like the ones defined in Eqs. (2) and (3), were simply calculated by setting $(E_\gamma, \mathbf{p}_\gamma) = (0, 0)$ (Fig. 12). The cuts in Fig. 5 had to be set to select rather than to remove elastic events, and the kinematic fit treated 9 instead of 12 parameters. Again the events with C.L.<0.2 were rejected (Fig. 8).

The important source for background was quasielastic scattering, i.e., scattering off a bound proton with the proton then knocked off the nucleus. Since ^{3}He has the smallest binding energy, the helium background is hardest to remove, and it was assumed that it was the only contribution surviving the kinematic fit. The carbon dummy target runs were used to calculate the helium contribution: The number of events b_j that passed with C.L.>0.2 (Fig. 8) was multiplied by 0.88 to correct for the small difference in the helium content of the carbon and the butanol target, and then entered into the likelihood fit as background. The background level was low (Table V), and the alternative assumption, that not helium but only carbon was its primary source, would have led to a 0.1 σ effect on the final result.

To combine the results from bremsstrahlung and elastic trigger runs, the sampling rate of the bremsstrahlung trigger was taken into account. The sampling factor (photon detector rate times gate width ≈ 0.006) was multiplied with beam flux and chamber efficiency to form the α_i of Eq. (11). Since the contribution of true three particle events to the photon trigger rate is negligibly small, no photon time-of-flight cuts were applied to remove the events with prompt photons.

The elastic scattering asymmetry is given in Fig. 13 and Table VI. It can be compared to phase shift predictions based on the KA84 phase shifts [29]. The eight data points fitted the phase shift calculations with a χ^2 of 7.8. Consequently the agreement with previous measurements at similar beam energies [30] is good. With the approximation $\beta_\pi \approx 0°$, the proton parameters are fixed by the pion scattering angle α_π, and no averaging over detector acceptances is needed before comparing.

V. DISCUSSION OF RESULTS

The bremsstrahlung analyzing power measurement was performed to obtain a less model dependent result

TABLE V. Analyzing power A as a function of photon energy. k_- and k_+ are the number of events found for positive and negative target polarization. b_- and b_+ are the corresponding number of background events. Beam flux α is in arbitrary units. Our result is compared to the MIT theory averaged over the detector acceptance ($\mu_\Delta = 1.6$, model I), and point calculations ($\alpha_\pi = 90°$, $\alpha_\gamma = -120°$, $\beta_\pi = \beta_\gamma = 0°$).

	E_γ	Events		Backgr.		Cross-section asymmetry		
	(MeV)	k_-	k_+	b_-	b_+	Experiment	MIT avg.	MIT pt.
1	27.5	159	155	12	5	0.21±0.13	0.08	0.10
2	42.5	141	102	3	6	−0.09±0.13	−0.04	−0.06
3	57.5	135	84	1	3	−0.24±0.14	−0.26	−0.27
4	72.5	100	52	2	0	−0.39±0.17	−0.49	−0.49
5	87.5	71	23	0	0	−0.78±0.21	−0.60	−0.59
6	102.5	64	18	0	0	−0.86±0.22	−0.52	−0.52
7	117.5	11	2	0	0	−1.11±0.44	−0.38	−0.36
Total		681	436	18	14			
Flux α		339	271					
Pol. P		−0.47	0.58					

for the magnetic dipole moment of the Δ. The difference between the two parametrizations of the $\pi N\Delta$ vertex function allowed from analyzing elastic scattering data with the isobar model leads to a systematic error of $\delta\mu_\Delta < 0.16\,\mu_p$, smaller than the experimental error of $\delta\mu_\Delta = 0.18\,\mu_p$. The result is independent of the upper limit on the photon energy, while the cross-section fit is not. As shown in Fig. 11 the cross section for the two parametrizations differ by ≈25%, while the asymmetries differ by only 6% at 60 MeV, where the sensitivity to μ_Δ is maximal. The model I parametrization is preferred, because it leads to a smaller difference between the bare and the dressed Δ mass. In Ref. [11] it is explicitly stated that the theoretical model becomes less certain when E_γ is comparable to $\Gamma_\Delta \approx 120$ MeV. From the relativistic extension of the MIT model no curves for our kinematics are available. However, for 298 MeV pion energy, a pion angle of 50.5° (UCLA geometry) and a coplanar photon at $\alpha_\gamma = -120°$ we found that Wittman's published curves [13] for $\mu_\Delta/\mu_p = 2.0$ and 2.3 agree quite well with the MIT model for photon energies below 80 MeV. For higher energies the curves diverge, in line with what the comparison of our data with the MIT model indicates, too.

In a recent article [31] the soft photon technique for calculating pion proton bremsstrahlung was extended to higher energies and μ_Δ radiation included. A reasonable fit to our cross-section data (11 data points in 10 MeV bins in photon energy, $55° < \Theta_\pi < 95°$) [14] was obtained with $\mu_\Delta = 1.70 \pm 0.09\,\mu_p$ ($\chi^2/n_D = 2.4$). Predictions for the asymmetry are not available. The fit to the UCLA data leads to $1.33 < \mu_{\Delta^{++}}/\mu_p < 1.51$. The overall agreement with the data is quoted as good, for the examples shown it is indeed the case. The predictions for our backward cross-section data, corresponding more closely to the geometry of this experiment are shown in Fig. 11. Taken at face value, these results are reassuring, but the discrepancy between the MIT model and this model is

TABLE VI. Elastic $\pi^+ p$ scattering analyzing powers at 298 MeV. α_π is the pion center-of-mass scattering angle. The scattering plane was perpendicular to the target field ($\beta_\pi \approx 0°$). The number of events for positive and negative target polarization and the number of surviving carbon target events are given. Beam flux α is in arbitrary units. The last column gives the phase shift prediction.

α_π (c.m.)	Events		Backgr.	Cross-section asymmetry	
(deg)	k_-	k_+	b	Experiment	KA84
87.5	5 883	5 742	23	0.438±0.039	0.435
92.5	8 165	7 431	53	0.372±0.034	0.444
97.5	7 665	7 186	51	0.393±0.035	0.412
102.5	7 116	6 117	47	0.319±0.033	0.334
107.5	8 599	6 868	24	0.244±0.028	0.223
112.5	9 357	6 399	42	0.095±0.020	0.109
117.5	12 581	8 007	65	0.028±0.015	0.015
122.5	12 798	7 409	74	−0.068±0.017	−0.050
Total	72 164	55 159	379		
Flux α	180	112	88		
Pol. P	−0.47	0.58			

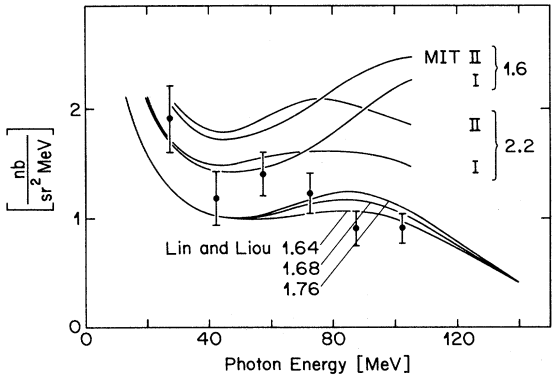

FIG. 11. Results of theoretical cross-section predictions for various values of μ_Δ/μ_p. Our measured cross section [14] [$75° < \alpha_\pi < 95°$, Fig. 3(b)] is compared to MIT predictions and to recent soft photon calculations for the same data by Lin and Liou [31].

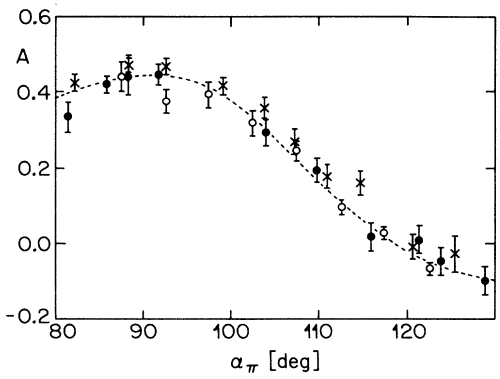

FIG. 13. Analyzing power A for $\pi^+ p$ elastic scattering versus pion center-of-mass scattering angle at 415 MeV/c. The dashed line is the KA84 prediction [29]. Our data (o) is compared to results from previous experiments by Dubal *et al.* (•) at 408 MeV/c, and Gorn (×) at 417 MeV/c [30].

still large, even at moderate photon energies. The new calculations seem to give a better fit to the high-energy data points. The theoretical articles however do not offer any clues as to what might cause these differences. Only for the UCLA data set [8] G6 (pion energy 298 MeV, photon angle $\alpha_\gamma = -140°$, $\beta_\gamma = -36°$, $\Theta_\pi = 50°$) all three calculations published curves, Wittman's [13] best fit curve for $2.0\,\mu_p$ is nearly identical with Lin and Liou [31] best fit curve for $1.5\mu_p$ and below 80 MeV also with the MIT [11] curve for 2.0 μ_p. This would indicate typically a 25% relative error contribution from the theoretical model, if the magnetic dipole moment is extracted from the cross-section data. The difference between the two parametrizations used in the MIT model is almost as large as the difference to the soft photon predictions for the cross section, but applied to asymmetry data only a 10% error contribution results for the magnetic moment. We therefore also expect that switching models will have a smaller effect for the asymmetry analysis. But it would certainly strengthen our conclusions if asymmetry predictions from all three calculations confirming our conjecture became available.

Awaiting these calculations, we conclude by observing that our result $\mu_\Delta/\mu_p = 1.62 \pm 0.18$ (expt) ± 0.16 (theor) is in good agreement with bag-model predictions. The naive, static constituent quark model gives:

$$\mu_p = \tfrac{4}{3}\mu_u - \tfrac{1}{3}\mu_d\,, \quad \mu_n = -\tfrac{1}{3}\mu_u + \tfrac{4}{3}\mu_d\,,$$

$$\mu_{\Delta^{++}} = 3\mu_u \approx 2\mu_p\,.$$

It was pointed out by Brown, Rho, and Vento [2] that the pion cloud contributions to the nucleon magnetic moments contain two-body terms ($\frac{6}{11}$ of the total cloud contribution), which cannot be absorbed in the quasiparticle moments of the naive quark model. Since the two-body contribution is antisymmetric in the quark spin and isospin indices, it has a nonvanishing expectation value only for the nucleon moments, but not for the moments of Δ, Λ, Σ, or Ξ. Measuring the Δ moment therefore determines the real quasiparticle moments without the two-body contribution, or vice versa the Δ^{++} moment should be smaller than what the naive quark model predicts by about 17 to 21% for values of a parameter δ between 0.4 and 0.5. δ is defined such that the quark-bag contributions to the isovector nucleon moments are $(1-\delta)$ times those given in the above formulas. Our experimental result would indicate $\delta \approx 0.4$, as suggested by the chiral bag model. For this value the equality $\mu_{\Sigma^-} = \mu_{\Xi^-} = \mu_\Lambda$ should hold, which is nearly fulfilled for Ξ^- and Λ.

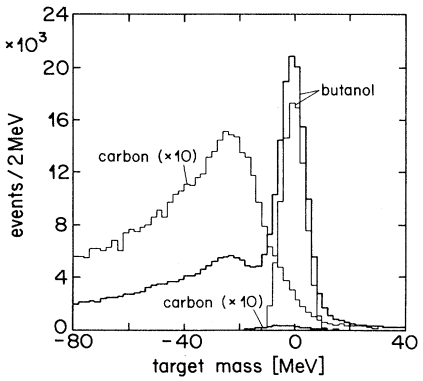

FIG. 12. Reconstructed target mass minus proton mass, $m_t - m_p$, for the πp system. For all bremsstrahlung triggers with a good pion and a proton, and for the accepted events with C.L.>0.2. The butanol is compared to the carbon. The carbon scale is magnified (×10).

ACKNOWLEDGMENTS

We would like to thank the Paul Scherrer Institute (formerly SIN) and its previous director, Professor J. P. Blaser, not only for providing the pions, but also for fa-

cilitating the experiment in many other ways. We thank Dr. Q. Ingram, Dr. R. Frosch, Dr. P. Weymuth, and Dr. L. van Elmbt for their help and Dr. S. Kumano for making his computer code available to us. The work was supported by the Swiss National Science Foundation and the Office of Energy Research, Division of Nuclear Physics of the Office of High Energy and Nuclear Physics of the U.S. Department of Energy under Contract No. DE-AT03-81ER4000 and the National Science Foundation under Grant No. PHY-8519381.

---

* Present address: PSI c/o ETH, CH-8093 Zürich, Switzerland.
† Present address: CERN, CH-1211 Genève 23, Switzerland.
‡ Present address: Elektrowatt Ingenieurunternehmungen, CH-8001 Zürich, Switzerland.
§ Present address: Institut für Mittelenergiephysik, ETH, CH-5232 Villigen PSI, Switzerland.
** Present address: Physikalisches Institut der Universität Heidelberg, D-6900 Heidelberg, Germany.
†† Present address: Physik-Institut der Universität Zürich, CH-8001 Zürich, Switzerland.

[1] M. A. B. Bég, B. W. Lee, and A. Pais, Phys. Rev. Lett. **13**, 514 (1964).
[2] G. E. Brown, M. Rho, and V. Vento, Phys. Lett. **97B** 423 (1980).
[3] L. A. Kondratyuk and L. A. Ponomarev, Yad. Fiz. **7**, 111 (1968) [Sov. J. Nucl. Phys. **7**, 82 (1968)]; V. I. Zakharov, L. A. Kondratyuk, and L. A. Ponomarev, *ibid.* **8**, 783 (1968) [**8**, 456 (1969)].
[4] J. D. Jackson, *Classical Electrodynamics*, 2nd ed. (Wiley, New York, 1975), Chap. 15, p. 701ff.
[5] B. M. K. Nefkens and D. I. Sober, Phys. Rev. D **14**, 2434 (1976).
[6] W. E. Fischer and P. Minkowski, Nucl. Phys. **B36**, 519 (1972); R. Baier, L. Pittner, and P. Urban, *ibid.* **B27**, 589 (1971).
[7] M. Arman *et al.*, Phys. Rev. Lett. **29**, 962 (1972); D. I. Sober *et al.*, Phys. Rev. D **11**, 1017 (1975); K. C. Leung *et al.*, *ibid.* **14**, 698 (1976).
[8] B. M. K. Nefkens *et al.*, Phys. Rev. D **18**, 3911 (1978).
[9] M. M. Musakhanov, Yad. Fiz. **19**, 630 (1974) [Sov. J. Nucl. Phys. **19**, 319 (1974)].
[10] P. Pascual and R. Tarrach, Nucl. Phys. **B134**, 133 (1978).
[11] E. J. Moniz, Nucl. Phys. **A374**, 557c (1982); L. Heller, S. Kumano, J. C. Martinez, and E. J. Moniz, Phys. Rev. C **35**, 718 (1987).
[12] We refer to the model of Ref. [11] as the MIT model, despite the fact that not all authors are from MIT, because S. Kumano, then at MIT, provided us with the computer code.
[13] R. Wittman, Phys. Rev. C **37**, 2075 (1988).
[14] C. A. Meyer *et al.*, Phys. Rev. D **38**, 754 (1988); C. A. Meyer, Ph.D. thesis, University of California, 1987.
[15] A. Bosshard *et al.*, Phys. Rev. Lett. **64**, 2619 (1990); A. Bosshard, Ph.D. thesis, University of Zürich, 1990.
[16] D. Besset *et al.*, Nucl. Instrum. Methods **184**, 365 (1981).
[17] J. C. Alder *et al.*, Nucl. Instrum. Methods **160**, 93 (1979).
[18] H. Wind, *Formulae and Methods in Experimental Data Evaluation* (CERN, Geneva, 1983), Vol 3.
[19] H. P. von Fellenberg, Ph.D. thesis, University of Zürich, 1977.
[20] G. S. Kyle *et al.*, Phys. Rev. Lett. **52**, 975 (1984); R. Stamminger, Ph.D. thesis, University of Erlangen, 1983.
[21] Let y_i be the initial measurements, such as the proton energy as measured from the ADC reading, and let η_i be the same quantity estimated with a kinematic fit. Then the so-called stretch functions (or "pulls") are defined as $z_i = y_i - \eta_i / \sqrt{\sigma_i^2 - (G_\eta^{-1})_{ii}}$, where the σ_i are the estimated errors of the y_i and the $(G_\eta^{-1})_{ii}$ are the squared errors of the fit, should be normally distributed around 0 with $\sigma = 1$. The $-$ in the denominator has to be replaced by a $+$ if the measurement y_i was treated as an unknown, unmeasured quantity in the fit. A systematic shift of a z_i indicates systematic errors in the initial measurements, a $\sigma \neq 1$ indicates errors in estimating the σ_i. The σ_i for proton energy was adjusted to normalize the z_i distribution. Thereby systematic errors in the σ_i of other quantities could have been compensated. That is why it is preferable to independently measure each σ_i that enters the kinematic fit.
[22] A. Bay *et al.*, Nucl. Instrum. Methods A **271**, 497 (1988); A. Bay, Ph.D. thesis, University of Lausanne, 1986.
[23] A. Bay *et al.*, Phys. Lett. B **174**, 445 (1986).
[24] A. G. Frodesen, O. Skjeggestad, and H. Tøfte, *Probability and Statistics in Particle Physics* (Universitetsforlaget, Bergen-Oslo-Tromsø, Norway, 1979).
[25] In the present experiment the positive spin direction n was pointing downwards, the target magnetic field was pointing upwards.
[26] MINUIT, function minimization and error analysis program, from CERN.
[27] S. Kumano, Ph.D. thesis, Massachusetts Institute of Technology, 1985; and private communication.
[28] F. E. Low, Phys. Rev. **110**, 974 (1958).
[29] R. Koch and E. Pietarinen, Nucl. Phys. **A366**, 331 (1980); H. M. Staudenmaier, University of Karlsruhe (private communication).
[30] L. Dubal *et al.*, Helv. Phys. Acta **50**, 815 (1977); W. Gorn, Lawrence Berkeley Laboratory Report No. LBL 1320, 1973 (unpublished).
[31] D. Lin and M. K. Liou, Phys. Rev. C **43**, R930 (1991).